

Supplementary Information

Developing colloidal nanoparticles for inkjet printing of devices with optical properties tuneable
from the UV to the NIR

*Jonathan S. Austin, Weitong Xiao, Feiran Wang, Nathan D. Cottam, Geoffrey Rivers, Ellie B. Ward, Tyler S. S. James, Christopher J. Tuck, Richard Hague, Weiling Luan, Oleg Makarovsky, and Lyudmila Turyanska**

Dr. J. S. Austin, Mr W. Xiao, Dr. F. Wang, Ms. E. B. Ward, Dr. G. Rivers, Prof. C. J. Tuck, Prof. R. Hague, and Dr L. Turyanska
Centre for Additive Manufacturing, Faculty of Engineering, University of Nottingham, Jubilee Campus, Nottingham, NG8 1BB, UK

Mr W. Xiao and Dr W. Luan
CPCIF Key Laboratory of Advanced Battery Systems and Safety, School of Mechanical and Power Engineering, East China University of Science and Technology, Shanghai 200237, China

Dr. N. D. Cottam, Dr. T. S. S. James and Dr. O. Makarovsky,
School of Physics and Astronomy, University of Nottingham, Nottingham, NG7 2RD, UK

SI1. Characterisation of Inks

TEM imaging of PbS QDs synthesized with DHLA-PEG₄₀₀-NH₂ capping ligands and a molar ratio Pb : S : L = 1 : 0.3 : 3 (**Figure S1a**) revealed an average QD diameter of $d = 3.0 \pm 1.0$ nm (**Figure S1b**). PL spectra of PbS QD films were measured with $\lambda_{\text{ex}} = 533$ nm (**Figure S1c**) and displayed a PL peak centred at $\lambda = 990$ nm and with FWHM of 160 nm. For all formulated inks, droplet formation was assessed using optical microscopy and contact angle measurements (**Figure S2**).

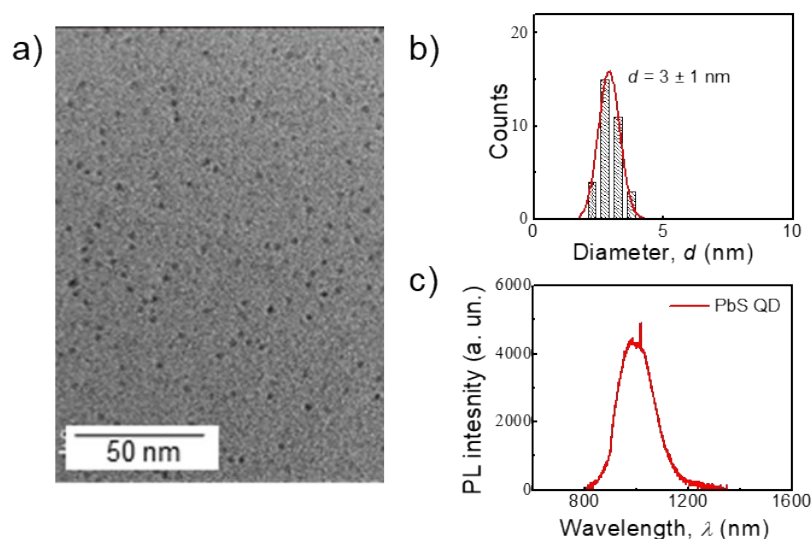


Figure S1. a) TEM image, b) size distribution histogram, and c) PL spectra of printed PbS QD film measured using $\lambda_{\text{ex}} = 530$ nm.

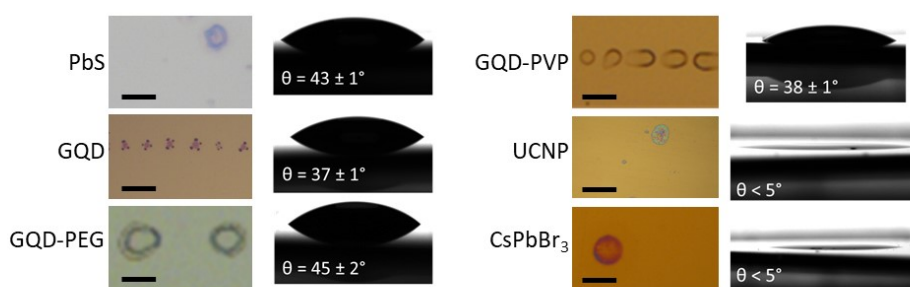


Figure S2. Optical microscope images of single droplets of each ink studied in this work printed onto Si/SiO₂ substrate. Scale bars represent 50 μm.

The best GQD films were achieved with the GQD-PVP ink, which achieved high quality prints on glass, Si/SiO₂ (**Figure S3a**), Kapton, and PEN substrates, however some non-uniformity was still revealed by PL mapping (**Figure S3b**). PL spectra of the GQD-PVP film displayed a large peak at $\lambda = 485$ nm and only a small shoulder at 610 nm (**Figure S3**, black line). The peak at $\lambda = 610$ nm is usually attributed to oxidation,³ hence, GQD oxidation is effectively suppressed by the addition of PVP.

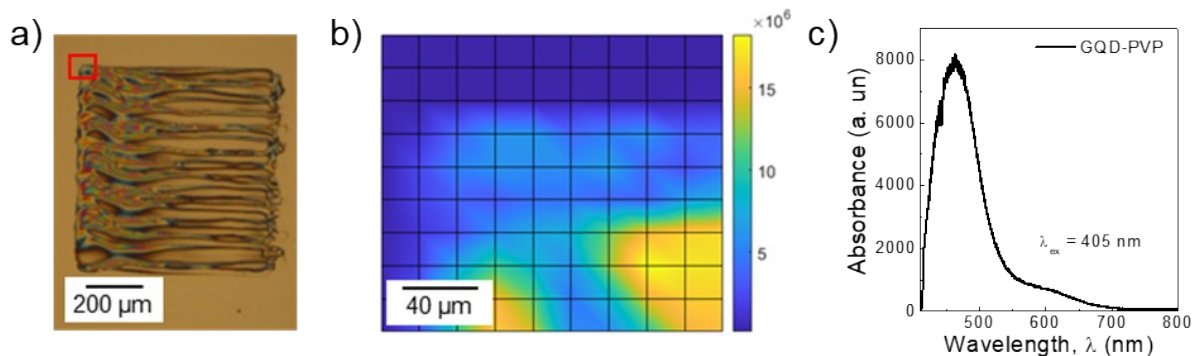


Figure S3. a) Optical image of 5 printed layers of GQD-PVP on Si/SiO₂, with red square indicating region of PL mapping. b) PL map ($\lambda_{\text{ex}} = 405$ nm). of printed GQD-PVP film. c) PL spectra GQD-PVP film. ($\lambda_{\text{ex}} = 405$ nm).

TEM imaging of β -NaYF₄: 20%Yb³⁺, 2%Er³⁺ UCNPs (**Figure S4a**) revealed an average UCNP diameter of $d = 18.8 \pm 1.7$ nm (**Figure S4b**). PL spectra of β -NaYF₄: 20%Yb³⁺, 2%Er³⁺ UCNP films were measured with $\lambda_{\text{ex}} = 980$ nm (**Figure S4c**), revealing green fluorescence and two main PL peaks centered at 540 nm and 654 nm, with narrow FWHM of 13 nm and 16 nm, respectively. PL spectra of β -NaYF₄: 2%Er³⁺ UCNP films were measured with $\lambda_{\text{ex}} = 980$ nm (**Figure S4c**), revealing orange fluorescence and different ratio of peak intensities.

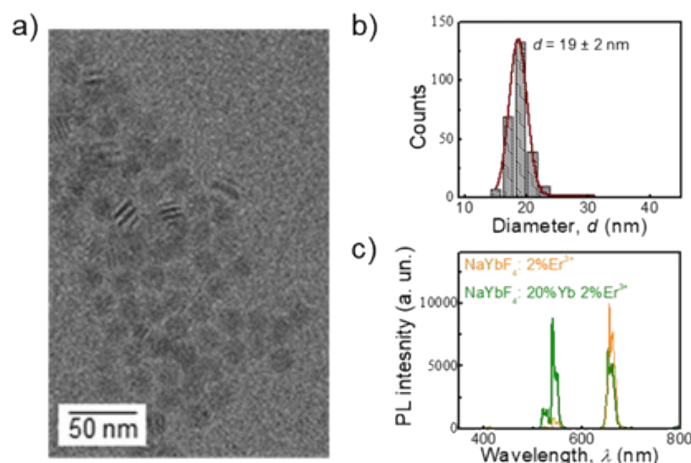


Figure S4. a) TEM image, b) size distribution histogram, and c) PL spectra of printed β -NaYF₄: 20%Yb³⁺, 2%Er³⁺ UCNP films measured using $\lambda_{\text{ex}} = 980$ nm.

Raman mapping was performed to investigate the quality of the printed UCNP films on the Si/SiO₂ substrate based on the peaks of the Raman spectra (**Figure S5d**) at 242, 295, 352 and 421 cm⁻¹ were characteristic for the UCNP,¹ and at 2800-3000 cm⁻¹ associated with C-H stretching vibrations of the organic solvents. Optical/microscopy images and high-resolution

Raman maps of organic signals (**Figure S5a-c**) confirmed that the uniformity of the film was significantly improved by increasing the number of printed layers. However, the UCNP's distribution in printed films was not obviously changed with increased number of printed layers (**Figure S5e**).

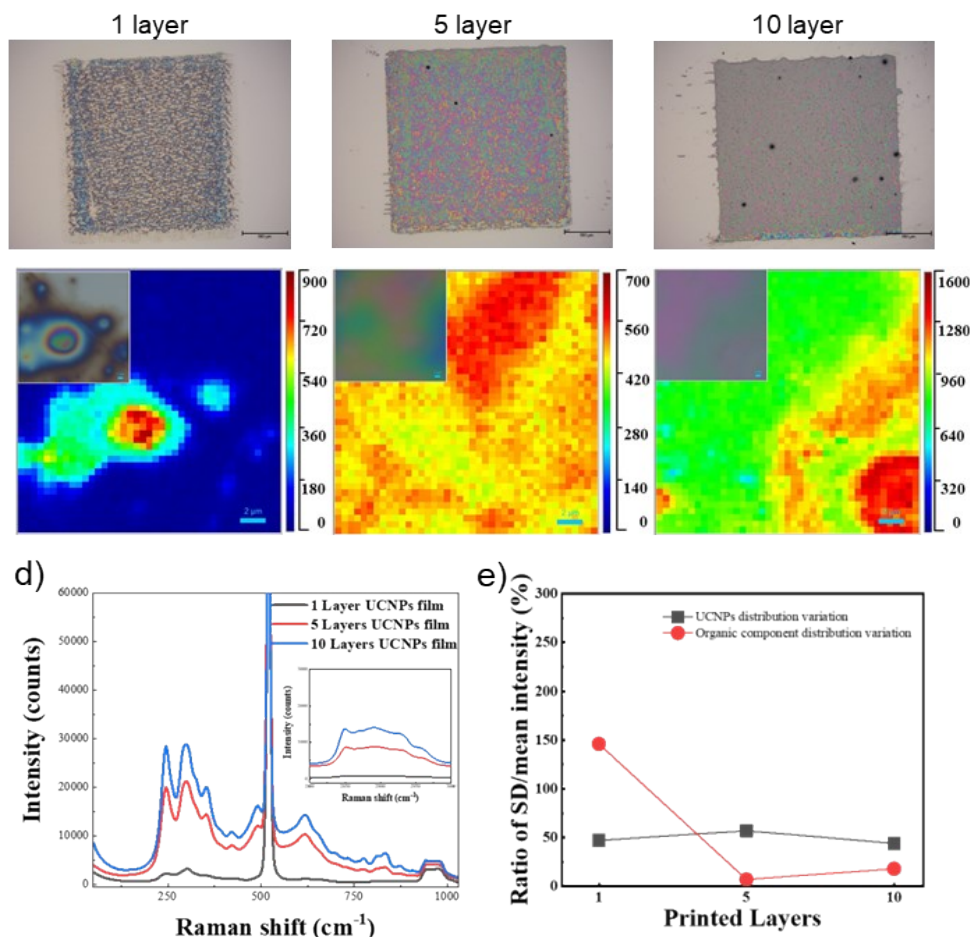


Figure S5 (first row) Optical images and (second row) Raman maps of organic signal distribution (intensity from 2800-3000 cm⁻¹) for printed UCNP's on Si/SiO₂ with: **a)** 1 printed layer, **b)** 5 printed layers, and **c)** 10 printed layers. **e)** Raman mean spectra of UCNP's films (200x200 μm) with different layer numbers on Si/SiO₂ substrate. Note: strong 520.7 cm⁻¹ signal belongs to standard Si (100) reference band. **f)** The ratio of standard deviation/mean intensity based on 20×20 μm Raman maps of different layer UCNP film. Black dot-line represent the UCNP's distribution variation, and the red dot-line represent the organic component distribution variation.

SI2. Characterisation of Devices

GQD ink, followed by GQD-PVP ink was deposited onto SLG via inkjet printing (**Figure S6a**). Before printing, the SLG had two Dirac points, one at $V_g \sim +80$ V (just above the V_g range measured), and another at $V_g = +10$ V (**Figure S6a**, black lines). After GQD and GQD-PVP deposition, an n-type shift was observed and Dirac points were located at $V_g = +7$, $+38$, and $+67$ V (**Figure S6a**, green lines). Unlike previous samples, hysteresis was unchanged after the deposition of GQD and GQD-PVP inks.

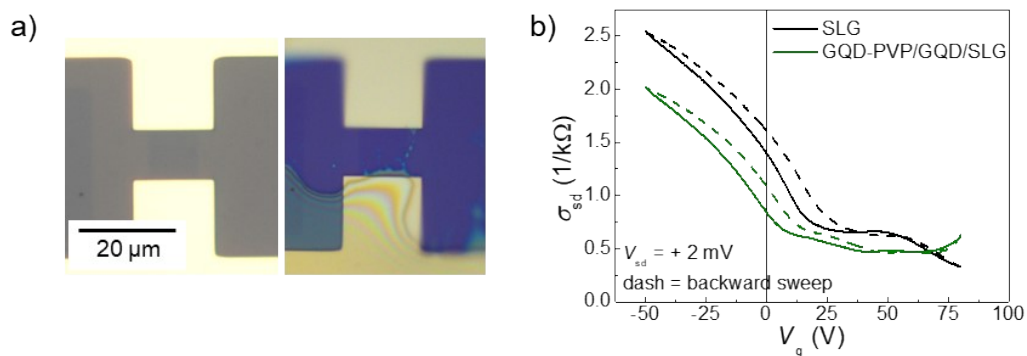


Figure S6. a) Optical images of SLG device before (left) and after (right) inkjet deposition of GQDs and GQD-PVP. **b)** $\sigma_{sd}(V_g)$ dependence of SLG before and after inkjet deposition of GQD and GQD-PVP. V_g is swept from -50 V to +80 (solid lines) and then back to -50 V (dashed lines) ($V_{sd} = 2$ mV, sweep rate = 0.17 V/s).

A drop of GQD ink was first deposited on SLG FETs and subsequently, a drop of GQD-PEG ink was deposited on top to fabricate a GQD-PEG/GQD/SLG device. During smaller V_g sweeps of ± 20 V instead of ± 50 V, no hysteresis was observed in GQD-PEG/GQD/SLG or in GQD/SLG devices (**Figure S7a**). The emergence of hysteresis in $\sigma_{sd}(V_g)$ at V_g sweeps at somewhere in the region between ± 20 V and ± 50 V, shows that there is an activation energy that must be overcome in order for charges to accumulate in the QDs. The $\sigma_{sd}(V_g)$ dependence for GQD-PEG/GQD/SLG device was changed by reducing V_g sweep speed to 0.013 V/s (**Figure S7b**), which is indicative of slow charge dynamics. Charge dynamics were further explored by AC electrical measurements (**Figure S7c**). The capacitance was approximately constant at $C \sim 16$ pF for all frequencies measured on SLG. After deposition of GQD and GQD-

PEG, the capacitance increased with decreasing frequency (**Figure S7c**). Hence, charges are only able to accumulate in the GQDs at low frequencies due to slow charge dynamics.

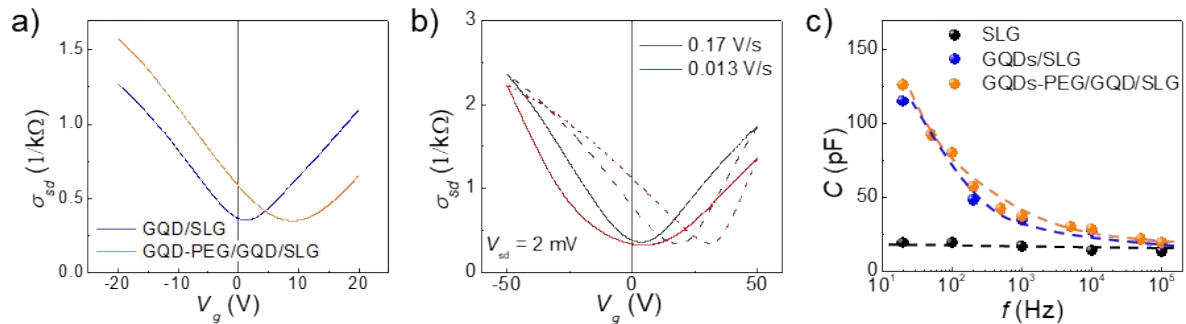


Figure S7. **a)** $\sigma_{sd}(V_g)$ dependence of GQDs/SLG and GQDs-PEG/GQD/SLG devices when V_g is swept from -20 V to +20 V (solid lines) and then back to -20 V (dashed lines) ($V_{sd} = 2$ mV, sweep rate = 0.17 V/s). **b)** $\sigma_{sd}(V_g)$ dependence of GQDs-PEG/GQD/SLG when V_g is swept from -50 V to +50 V (solid lines) and then back to -50 V (dashed lines) with a sweep rate of 0.17 V/s (grey curves) and 0.013 V/s (red curve) ($V_{sd} = 2$ mV). **c)** Capacitance of SLG, GQD/SLG, and GQD-PEG/GQD/SLG devices as a function of frequency, measured between the gate and the source-drain contacts (dashed lines are a guide to the eye).

SLG FETs were decorated with a single drop of GQD (**Figure S8a**), PbS QD (**Figure S8b**), and UCNP (**Figure S8c**) ink. The inks based on non-polar solvent (UCNPs) displayed the best wetting, and thus achieved the greatest coverage onto the hydrophobic SLG. All measured devices displayed recoverable ON/OFF responses. The GQD/SLG device had response times of $\tau_{ON} = 50$ s and $\tau_{OFF} = 800$ s under $\lambda_{ex} = 405$ nm (**Figure S8a**), the PbS QD/SLG device had response times of $\tau_{ON} = 40$ s and $\tau_{OFF} = 300$ s under $\lambda_{ex} = 808$ nm (**Figure S8b**), and the UCNP/SLG device had response times of $\tau_{ON} = 20$ s and $\tau_{OFF} = 20$ s under $\lambda_{ex} = 970$ nm (**Figure S8c**).

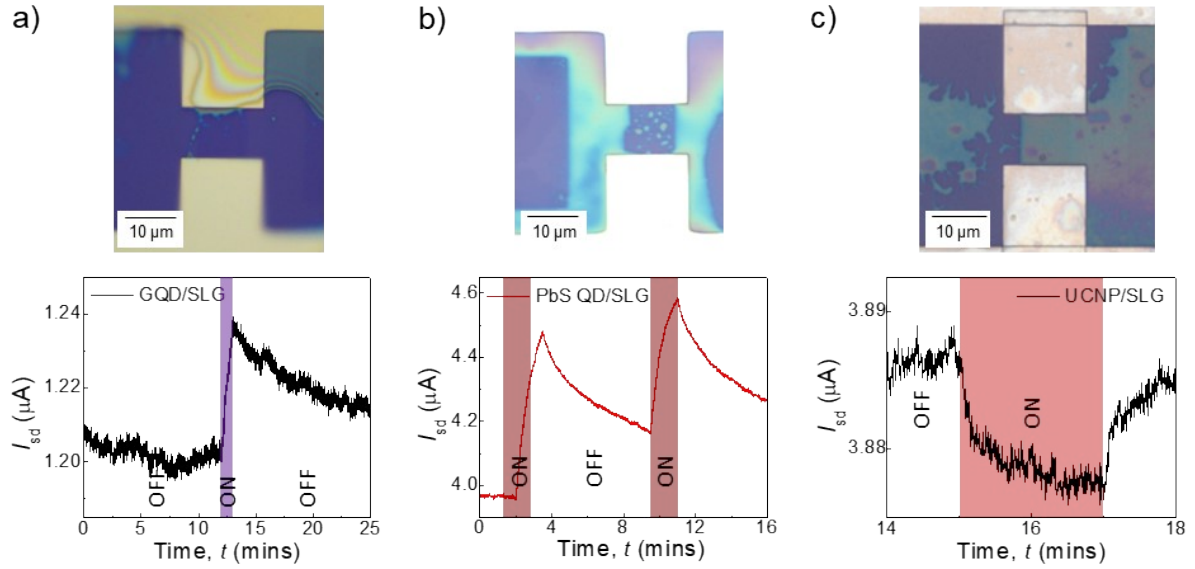


Figure S8. (top row) Optical images and (bottom row) temporal ON/OFF responses of **a)** GQD/SLG device ($V_{sd} = 2$ mV, $V_g = 0$ V, $\lambda_{ex} = 405$ nm, $P = 56.6$ W/m²), **b)** PbS QD/SLG device ($V_{sd} = 4$ mV, $V_g = 0$ V, $\lambda_{ex} = 808$ nm, $P = 1800$ W/m²), and **c)** UCNP/SLG device ($V_{sd} = 2$ mV, $V_g = 0$ V, $\lambda_{ex} = 970$ nm, $P = 290$ W/m²).

References

- 1 S. Wilhelm, T. Hirsch, W. M. Patterson, E. Scheucher, T. Mayr and O. S. Wolfbeis, *Theranostics*, 2013, **3**, 239–248.
- 2 Z. Gan, H. Xu and Y. Fu, *J. Phys. Chem. C*, 2016, **120**, 29432–29438.
- 3 S. Jeong, R. L. Pinals, B. Dharmadhikari, H. Song, A. Kalluri, D. Debnath, Q. Wu, M. H. Ham, P. Patra and M. P. Landry, *Sci. Rep.*, 2020, **10**, 7074.